



## Dissolution Behavior of Al<sub>2</sub>CuMg (S Phase) in Chloride and Chromate Conversion Coating Solutions

Yuhchae Yoon and R. G. Buchheit<sup>z</sup>

Fontana Corrosion Center, Department of Materials Science and Engineering, The Ohio State University,  
Columbus, Ohio 43210, USA

The dissolution rate and Cu surface enrichment of sputter-deposited Al<sub>2</sub>CuMg thin films exposed to 0.5 M NaCl solutions and chromate conversion coating solutions has been characterized. Dissolution rates were measured using an electrochemical quartz crystal microbalance, and Cu surface enrichment was characterized by energy-dispersive spectroscopy (EDS). Surface morphology and Volta potential were characterized by scanning probe microscopy. In 0.5 M NaCl solutions, Al<sub>2</sub>CuMg dissolves rapidly by dealloying, forming a passivating Cu-rich surface layer. Upon layer breakdown a dissolution rate of about 0.08 μg/cm<sup>2</sup> s was observed. In chromate conversion coating baths, Al<sub>2</sub>CuMg demonstrated a net mass loss rate, which included mass loss from dissolution and mass gain from film formation. Cu surface enrichment was not detected after conversion coating. By comparison, pure Al thin films exhibited a net mass gain under similar conditions. Al<sub>2</sub>CuMg samples that were first chromate conversion coated and then exposed to 0.5 M NaCl solution exhibited low dissolution rates, 0.001 μg/cm<sup>2</sup> s, suggesting that the film formed in the conversion bath was somewhat protective. EDS showed that Cu enrichment occurred on conversion-coated Al<sub>2</sub>CuMg during exposure to 0.5 M NaCl, indicating that conversion coatings on Al<sub>2</sub>CuMg cannot completely suppress Cu surface enrichment, Cu redistribution, and deposition corrosion phenomena.

© 2006 The Electrochemical Society. [DOI: 10.1149/1.2177005] All rights reserved.

Manuscript submitted October 28, 2004; revised manuscript received November 15, 2005. Available electronically March 9, 2006.

The Al<sub>2</sub>CuMg intermetallic compound, sometimes referred to as the S phase, is present in Al–Cu–Mg and Al–Zn–Mg–Cu alloys as coarse 0.5–10 μm diameter constituent particles and as fine, nanometer-sized, lath-shaped precipitates.<sup>1–15</sup> Al<sub>2</sub>CuMg is electrochemically active, and constituent particles of this compound significantly affect localized corrosion and surface finishing of alloys that contain them.<sup>1–13,16</sup>

Direct electrochemical measurements of Al<sub>2</sub>CuMg synthesized in bulk form show that the phase exhibits corrosion potentials in the range of –0.88 to –0.93 V<sub>SCE</sub> in neutral chloride solutions.<sup>17</sup> This makes the phase active with respect to the surrounding matrix. Under free corrosion conditions, the phase dissolves at an appreciable rate by dealloying. Dealloying can significantly ennoble the phase as the dissolving particle surface becomes enriched with Cu. Dealloyed particles can catalyze oxygen reduction, leading to the development of local alkalinity and cathodic corrosion of the surrounding matrix.<sup>16</sup>

In some cases the dealloyed Al<sub>2</sub>CuMg remnant can release Cu ions at potentials well below the reversible potential for Cu that might be estimated from the Nernst equation.<sup>13</sup> Cu ion release involves formation and detachment of metallic Cu clusters from a coarsening dealloyed particle followed by direct oxidation of the Cu clusters once they are physically detached from the Al<sub>2</sub>CuMg particle and the alloy substrate.<sup>12</sup> Once detached, Cu clusters are electrically isolated from the alloy substrate and can move to more positive potentials where they are oxidized to Cu ions that can plate elsewhere on the alloy surface and lead to deposition corrosion.<sup>18</sup>

In Al–Cu–Mg alloy 2024-T3, Al<sub>2</sub>CuMg particles have been observed to interfere with the formation of chromate conversion coatings (CCCs). Raman scattering at 860 cm<sup>–1</sup> is indicative of Cr<sup>3+</sup>–O–Cr<sup>6+</sup> bonding in CCCs, and the intensity of the band is directly proportional to CCC thickness. High-spatial-resolution microfocal Raman microscopy has shown that CCCs are thinner on coarse constituent Al<sub>2</sub>CuMg particles in 2024-T3.<sup>19</sup>

Al<sub>2</sub>CuMg particles are also present in Al–Zn–Mg–Cu alloy 7075. Localized corrosion on chromate conversion coated 7075 substrates after exposure to aerated chloride solutions is commonly associated with Al<sub>2</sub>CuMg particles present in the alloy.<sup>15</sup>

The objective of this paper is to present results comparing the reactivity of Al<sub>2</sub>CuMg before, during, and after chromate conversion coating. The experimental approach used was based on an electrochemical quartz crystal microbalance measurement of thin-film

compositional analogs of Al<sub>2</sub>CuMg. Interpretation of observed mass changes was aided by open-circuit potential measurements, measurements of sample composition by energy-dispersive spectroscopy, and characterization of surface morphology and Volta potential by scanning probe microscopy.

### Experimental

**Thin-film sample preparation.**—Sputter deposition was used to prepare Al<sub>2</sub>CuMg and pure Al samples for this study. A target with a composition of 50Al–25Cu–25Mg (in atom %) was used to prepare Al<sub>2</sub>CuMg samples. A 99.99% pure Al target was used to prepare Al thin films. The targets were obtained from a commercial source (PlasmaMaterials, Inc., Livermore, CA) and were 7.62 mm in diameter and 1 mm in thickness. Deposition was carried out at nominally ambient temperatures using dc/radio frequency (rf) sputtering (Denton Discovery® 18 System) in Ar gas at a base pressure of 2 × 10<sup>–7</sup> Torr. The accelerating voltage and ion current were maintained at 0.5 kV and 0.65 A, giving a deposition rate of 0.69 nm/s. To achieve a uniform thickness and composition in the samples, the substrate platen was rotated during deposition. Films were deposited onto Si wafers for electrochemical testing, or on 10-MHz AT-cut quartz crystals for microbalance experiments. The thickness of the sputtered thin films was determined by surface profilometry (Veeco: Dektak<sup>3</sup>ST). Films deposited on Si were about 2 μm thick while those deposited on quartz were about 500 nm in thickness. After deposition, the compositions of the Al<sub>2</sub>CuMg thin films were measured using energy-dispersive spectroscopy (EDS). The nominal compositions of the Al<sub>2</sub>CuMg samples ranged from 55Al–21Cu–24Mg to 56Al–22Cu–22Mg. No impurities (e.g., Fe or Si) were detected in EDS measurements of the pure Al films.

**Thin films on quartz substrates.**—For microbalance measurements, thin films were deposited on 10-MHz AT-cut quartz crystal substrates (International Crystal Manufacturing Co, Inc.). Prior to film deposition, crystals were cleaned by sonication in methanol and acetone for 3 min in each solution. The crystals were then rinsed with distilled water and carefully dried with Ar gas to remove any dust. After deposition, the crystal was mounted on a holder with the deposited film facing the solution. A three-electrode cell was used in which Pt was used as a counter electrode, and a saturated calomel electrode (SCE) was used as a reference electrode.

**Electrochemical quartz crystal microbalance measurements.**—The electrochemical quartz crystal microbalance (EQCM) technique is based on the measurement of a change in the resonant

<sup>z</sup> E-mail: buchheit.8@osu.edu

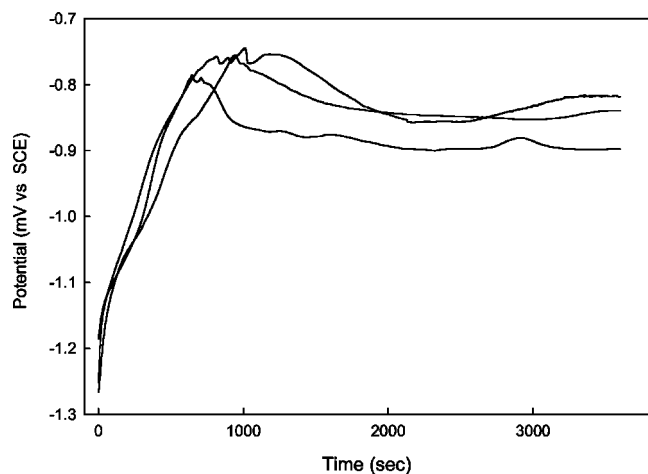


Figure 1. OCP vs time traces of  $\text{Al}_2\text{CuMg}$  in aerated 0.5 M NaCl.

frequency of a piezoelectric quartz crystal due to a change in the mass of a thin metal film deposited on it. The EQCM system used in these experiments consisted of an electrochemical microbalance (EQCN-900, Elchema), a frequency scanner (EQCN 906, Elchema), and a potentiostat (PS-605, Elchema). EQCM measurements were carried out in a Faraday cage to minimize electromagnetic interference. The change in resonant frequency ( $\Delta f$ ) was measured and converted to a mass change ( $\Delta m$ ) using the Sauerbrey equation.<sup>20</sup> At the same time, the potential was monitored using a potentiostat. According to the Sauerbrey equation, the relationship between resonant frequency change,  $\Delta f$ , and mass change,  $\Delta m$ , is linear<sup>20</sup>

$$\Delta f = -K_f \Delta m \quad [1]$$

where

$$K_f = \frac{2f^2}{A \cdot \sqrt{\mu_q \rho_q}} \quad [2]$$

The coefficient,  $K_f$ , depends on the square of the resonant frequency,  $f$ , of the quartz crystal and thin-film deposit prior to any mass change, the density of quartz,  $\rho_q$ , the shear modulus of the quartz,  $\mu_q$ , and the electrode surface area,  $A$ . In these experiments, a value of  $0.213 \text{ Hz cm}^2/\text{ng}$  was used for  $K_f$  to convert  $\Delta f$  to  $\Delta m$ . This value was determined empirically by measuring  $\Delta f$  during electrodeposition of Cu from a 0.05 M  $\text{CuSO}_4$  plus 0.05 M  $\text{H}_2\text{SO}_4$  solution. The quantity  $\Delta m$  was calculated using Faraday's law, assuming 100% deposition efficiency of a two-electron Cu reduction process. This value of  $K_f$  is in good agreement with a value of  $0.226 \text{ Hz cm}^2/\text{ng}$  calculated from Eq. 2.

**Chromate conversion coating.**— CCCs were applied by simple immersion of the various samples at their respective open-circuit potentials. Coating was carried out using Alodine 1200S conversion coating bath formulation. The chemistry of the bath as given in the manufacturer's specifications (Henkel Surface Finishing Technologies, North America, Madison Heights, MI) is 3.95–4.74 g/L  $\text{CrO}_3$ , 0.79–2.37 g/L  $\text{K}_3\text{Fe}(\text{CN})_6$ , 0.79–2.37 g/L  $\text{KBF}_4$ , 0.08–0.79 g/L NaF, and 0.08–0.79 g/L  $\text{K}_2\text{ZrF}_6$ .<sup>21</sup>

### Results and Discussion

**Reactivity of  $\text{Al}_2\text{CuMg}$  in 0.5 M NaCl.**— Figure 1 shows the evolution of the open-circuit potential (OCP) of several  $\text{Al}_2\text{CuMg}$  samples over 1 h during immersion in aerated 0.5 M NaCl. The OCP variation was reproducible and was characterized by an initial transient during which the OCP increased rapidly. After this transient, the OCP was considerably more stable. The OCP in the stable region ranged from  $-860$  to  $-760 \text{ mV}_{\text{SCE}}$ , which is slightly more noble than the OCP range reported for this phase in the literature.<sup>22</sup>

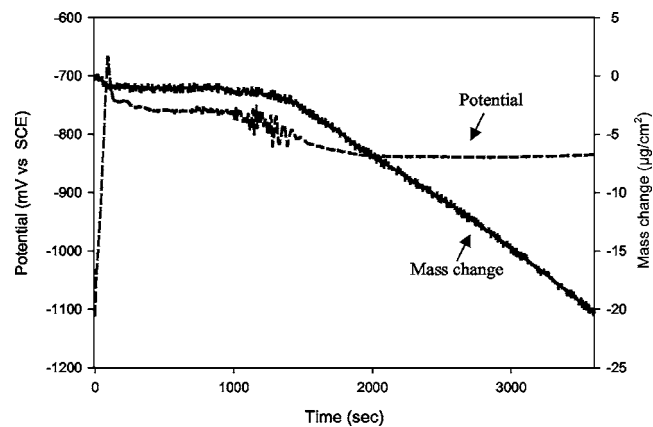


Figure 2. OCP and mass change of  $\text{Al}_2\text{CuMg}$  in aerated 0.5 M NaCl.

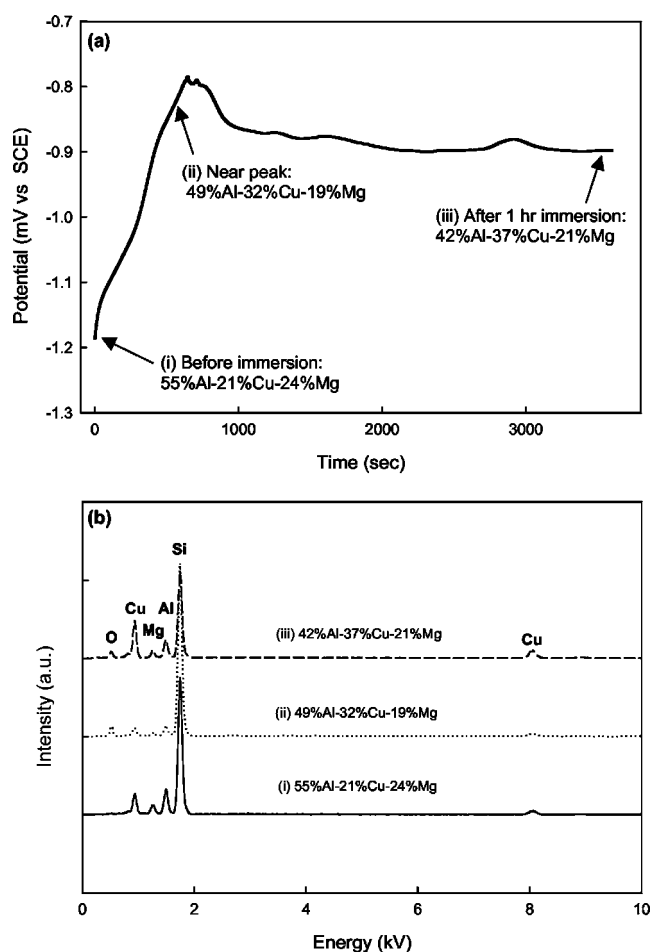
Figure 2 shows an OCP vs time record and the corresponding mass loss during an EQCM measurement of  $\text{Al}_2\text{CuMg}$  in 0.5 M NaCl solution. In this particular experiment the initial OCP transient was accompanied by a small decrease in mass. This particular transient was shorter than those shown in Fig. 1 but is believed to be a natural variation of the initial dissolution process. After about 1000 s of exposure, there is a slight decrease in OCP and the onset of stable dissolution at a rate of about  $0.08 \mu\text{g}/\text{cm}^2 \text{ s}$ . This slight decrease in OCP after the initial OCP transient can be recognized in each of the OCP vs time records in Fig. 1, suggesting that the regular open-circuit dissolution behavior  $\text{Al}_2\text{CuMg}$  in thin-film form is characterized by an initial episode of transient dissolution, temporary passivation, and a second episode of stable dissolution that does not lead to the formation of a protective film within the time frame of these experiments.

Figure 3 shows EDS spectra collected from  $\text{Al}_2\text{CuMg}$  samples withdrawn from solution after 800 and 3600 s of immersion in solution. A spectrum from an unexposed sample is also shown. Prior to analysis, exposed samples were rinsed with deionized water and air dried immediately upon withdrawal from solution. The EDS spectra indicate a progressive increase in Cu, suggesting dissolution by dealloying.<sup>13</sup> The first episode of dealloying produces a somewhat protective Cu-rich surface layer on the electrode that ennobles the OCP. With time (often a short time as suggested by Fig. 1) this layer breaks down, leading to a slight decrease in OCP and the onset of stable dissolution.

**Reactivity of  $\text{Al}_2\text{CuMg}$  during CCC formation.**— Conversion coatings were formed on  $\text{Al}_2\text{CuMg}$  and pure Al samples in a bath comprised of  $\text{CrO}_3$ ,  $\text{K}_3\text{Fe}(\text{CN})_6$ , NaF,  $\text{KBF}_4$ , and  $\text{K}_2\text{ZrF}_6$ . Samples were immersed for 3 min, which is about the maximum contact time used for the formation of chromate conversion coatings in practice. During immersion in the coating bath, samples were assumed to experience some amount of mass loss from dissolution and some amount of mass gain due to coating deposition. Measured mass changes were therefore taken to be net values comprising both components.

In the conversion coating bath over the span of 3 min, the OCP of  $\text{Al}_2\text{CuMg}$  increased by about 50 mV while sustaining net mass loss rate of  $0.007 \mu\text{g}/\text{cm}^2 \text{ s}$  (averaged over the time of immersion) (Fig. 4). During coating, the rate of net mass loss decreased slightly with time. Figure 2 indicates that  $\text{Al}_2\text{CuMg}$  can sustain a relatively high and stable rate of dissolution. Therefore the decreasing mass loss rate in Fig. 4 suggests the formation of a surface layer with increasing protectiveness.

Pure Al thin films gained mass during immersion in the conversion coating bath, resulting in a nominal mass gain rate of about  $0.003 \mu\text{g}/\text{cm}^2 \text{ s}$  (Fig. 5). Although the dissolution rates of Al and  $\text{Al}_2\text{CuMg}$  are not expected to be equal, it is not unreasonable to



**Figure 3.** OCP vs time (a), and sample compositions after selected immersion times for  $\text{Al}_2\text{CuMg}$  (b) exposed to 0.5 M NaCl solution. EDS spectra of  $\text{Al}_2\text{CuMg}$  in different immersion times. The intensities are offset vertically by 2000 counts.

conclude that the film formation rate on pure Al is greater than that on  $\text{Al}_2\text{CuMg}$ , resulting in much thicker chromate films on Al over the same length of immersion time in the coating bath.

The CCC formation on  $\text{Al}_2\text{CuMg}$  samples in this study was not carried out at the OCP of an Al alloy (e.g., 2024-T3) in the conversion coating bath. However, the results here are consistent with the

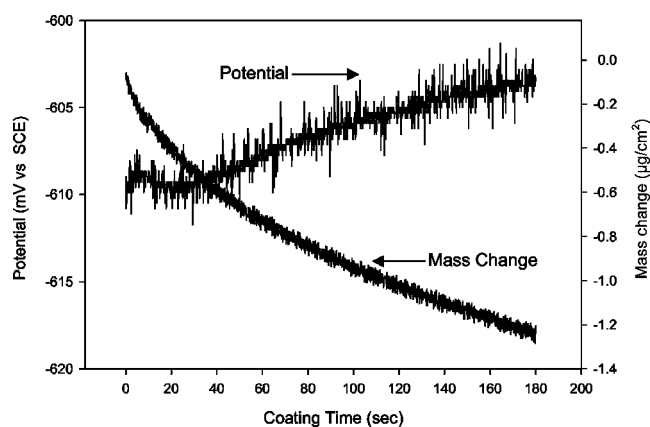


**Figure 4.** Variations in OCP and sample mass for  $\text{Al}_2\text{CuMg}$  during a 3-min exposure to a CCC bath.

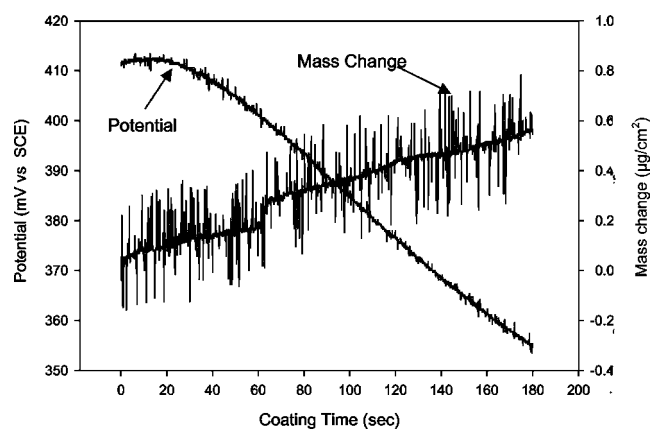


**Figure 5.** Variations in OCP and sample mass for pure Al during a 3-min exposure to a CCC bath.

observations of others, showing that conversion coatings are thicker on Al-rich matrix phase of Al alloys than on  $\text{Al}_2\text{CuMg}$  intermetallic particles.<sup>15,19,23</sup>

*Reactivity of  $\text{Al}_2\text{CuMg}$  after CCC formation.*—The  $5 \times 5 \mu\text{m}$  surface height and Volta potential maps of  $\text{Al}_2\text{CuMg}$  thin films in Fig. 6 show the differences in surface morphology and Volta potential distribution before and after application of a 3-min CCC. Before CCC formation, the root-mean-square (rms) roughness was about 2.63 nm. The morphology of the surface was characterized by compact mass nanometer-diameter nodules. The Volta potential map showed no contrast, even at nodule locations, suggesting no compositional heterogeneity at this length scale.

After application of the CCC, the surface roughness was increased slightly to 3.46 nm rms. Contrast variations in the surface height map showed elevated domains several micrometers in diameter separated by narrow valleys in morphology indicative of shrinkage cracks, which are commonly observed in air-dried CCCs.<sup>24</sup> The Volta potential map showed that surface potential was slightly elevated in the depressed, crack-like regions on the surface.

Combined OCP/EQCM measurements of the conversion-coated  $\text{Al}_2\text{CuMg}$  sample exposed to aerated 0.5 M NaCl solutions (dried

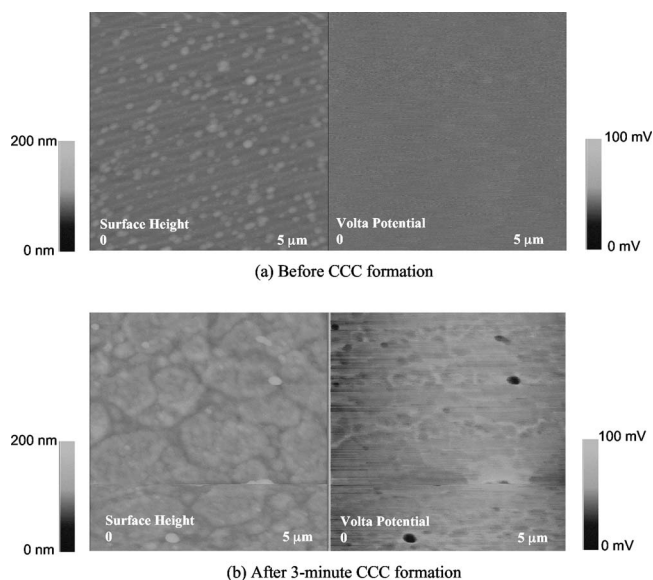


**Figure 6.** Surface height and Volta potential maps for  $\text{Al}_2\text{CuMg}$  before (a) and after (b) chromate conversion coating.

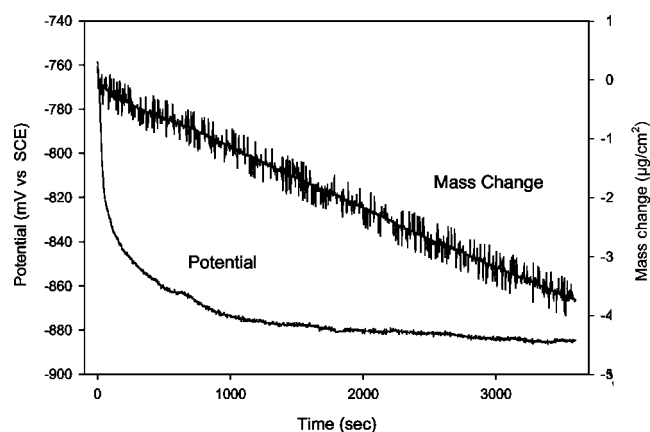


**Figure 7.** Variations in OCP and sample mass for  $\text{Al}_2\text{CuMg}$  conversion coated for 3 min then exposed to aerated 0.5 M NaCl solution.

for 24 h before immersion) are shown in Fig. 7. During these exposures, the OCP rapidly decreased to a value characteristic of  $\text{Al}_2\text{CuMg}$  without a conversion coating; however, the nominal mass loss rate was reduced by the presence of the coating to a value of about  $0.001 \mu\text{g}/\text{cm}^2 \text{ s}$ . This mass loss rate is more than two orders of magnitude lower than that of uncoated  $\text{Al}_2\text{CuMg}$ . While  $\text{Al}_2\text{CuMg}$  forms a thinner and presumably inferior chromate conversion coating, the coating that does form inhibits dissolution of  $\text{Al}_2\text{CuMg}$  to an appreciable extent.

**General observations.**— Table I summarizes mass loss rates for the thin film Al and  $\text{Al}_2\text{CuMg}$  samples in these experiments. Two mass loss rates are reported for uncoated  $\text{Al}_2\text{CuMg}$  in 0.5 M NaCl solution, reflecting the active and passive behaviors demonstrated by the phase after the initial OCP transient. Mass loss rates are much lower for  $\text{Al}_2\text{CuMg}$  in the conversion coating bath than in 0.5 M NaCl but much greater than pure Al, which gains mass during conversion coating. The absolute dissolution rate of  $\text{Al}_2\text{CuMg}$  in a conversion coating bath is likely to be greater than that indicated in the table, because this rate reflects the combination of mass gain from coating formation and mass loss from dissolution. With increased time, conversion coating slows but does not stop  $\text{Al}_2\text{CuMg}$  dissolution. How the dissolution rate of  $\text{Al}_2\text{CuMg}$  compares with that of the conversion-coated matrix phase in Al–Cu–Mg and Al–Zn–Mg–Cu alloys has not been established with certainty; however, it has been observed that breakdown of conversion-coated 7075 and 7475 alloy surfaces is usually associated with  $\text{Al}_2\text{CuMg}$  particles, indicating a less protective, and perhaps thinner coating at those sites on the alloy surface.<sup>15</sup>

EDS measurements shown in Fig. 8 indicate that Cu is not strongly enriched in  $\text{Al}_2\text{CuMg}$  during CCC. This is probably due to the lower dissolution rate of the phase in the bath and the comparatively short duration of the immersion. Cu enrichment of conversion-coated  $\text{Al}_2\text{CuMg}$  during exposure to aerated 0.5 M NaCl

**Table I.** Dissolution rates of thin-film analog of  $\text{Al}_2\text{CuMg}$  in different conditions.

Material and environment	Net dissolution rate ( $\mu\text{g}/\text{cm}^2 \text{ s}$ )
Bare $\text{Al}_2\text{CuMg}$ at OCP in aerated 0.5 M NaCl	
Active	-0.08
Passive	0
$\text{Al}_2\text{CuMg}$ in a CCC bath	-0.007
Pure Al in a CCC bath	+0.003
Conversion-coated $\text{Al}_2\text{CuMg}$ at OCP in 0.5 M NaCl	-0.001

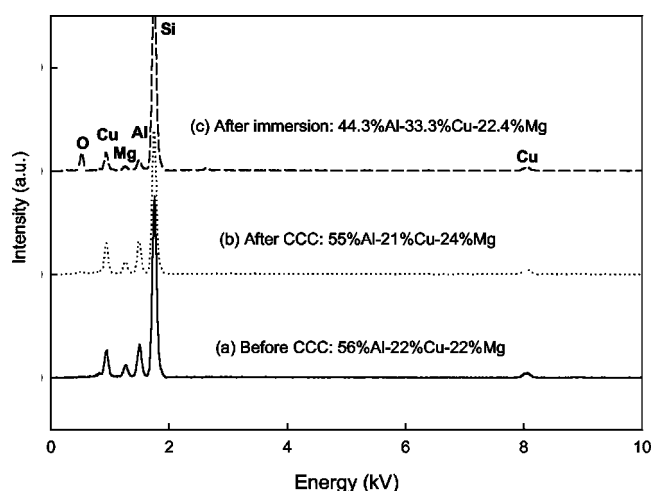


**Figure 8.** EDS spectra of  $\text{Al}_2\text{CuMg}$  before (a) and after (b) CCC, and an EDS spectrum of a conversion-coated  $\text{Al}_2\text{CuMg}$  sample after exposure to 0.5 M NaCl solution for 1 h (c). Spectra are offset vertically by 2000 counts.

solution was found to be appreciable. This suggests that CCCs may not completely suppress Cu enrichment and redistribution phenomena or the attendant deposition corrosion susceptibility in Al alloys containing  $\text{Al}_2\text{CuMg}$  particles.<sup>13</sup>

### Conclusion

In 0.5 M NaCl solutions under free corrosion conditions, EQCM, OCP, and EDS measurements of  $\text{Al}_2\text{CuMg}$  samples indicates that the phase is subject to dissolution by dealloying, leading to the formation of a Cu-rich surface layer that temporarily passivates the phase. Subsequently, this layer spontaneously breaks down, leading to continued, steady dissolution in the form of dealloying.

In a conversion coating bath,  $\text{Al}_2\text{CuMg}$  mass loss due to dissolution exceeds mass gain due to coating formation. This is in contrast to the behavior of pure Al where mass gain by coating formation exceeds mass loss due to dissolution. These findings are generally consistent with observations of coatings formed on Al alloys, which show that the coatings formed on  $\text{Al}_2\text{CuMg}$  particles are thinner and potentially less protective than those formed on the surrounding matrix phase.<sup>15,19,23</sup>

Mass loss rates of conversion-coated  $\text{Al}_2\text{CuMg}$  show that the coating that does form reduces the dissolution rate by about two orders of magnitude during exposure to aerated chloride solutions but does not suppress Cu enrichment of the phase and may not suppress deposition corrosion involving redistributed Cu.

### Acknowledgments

This work was supported by the Strategic Environmental Research and Development Program under contract no. DAC72-99-C-0002. The authors appreciate thin-film preparation by and valuable discussions with Jiho Kang and Professor Jerry Frankel.

The Ohio State University assisted in meeting the publication costs of this article.

### References

1. A. Kolics, A. S. Besing, and A. Wieckowski, *J. Electrochem. Soc.*, **148**, B322 (2001).
2. A. Kolics, A. S. Besing, P. Baradlai, and A. Wieckowski, *J. Electrochem. Soc.*, **150**, B512 (2003).
3. D. Q. Zhu and W. J. van Ooij, *Corros. Sci.*, **45**, 2163 (2003).
4. M. H. Shao, Y. Fu, R. G. Hu, and C. J. Lin, *Acta Phys. Sin.*, **18**, 350 (2002).
5. M. H. Shao, Y. Fu, R. G. Hu, and C. J. Lin, *Mater. Sci. Eng., A*, **344**, 323 (2003).
6. M. B. Vukmirovic, N. Dimitrov, and K. Sieradzki, *J. Electrochem. Soc.*, **149**, B428 (2002).
7. G. M. Brown and K. Kobayashi, *J. Electrochem. Soc.*, **148**, B457 (2001).
8. N. Dimitrov, J. A. Mann, and K. Sieradzki, *J. Electrochem. Soc.*, **146**, 98 (1999).
9. N. Dimitrov, J. A. Mann, M. Vukirovic, and K. Sieradzki, *J. Electrochem. Soc.*,

- 147**, 3283 (2000).
10. V. Guillaumin and G. Mankowski, *Corros. Sci.*, **41**, 421 (1999).
  11. R. G. Buchheit, *J. Appl. Electrochem.*, **28**, 503 (1998).
  12. R. G. Buchheit, R. P. Grant, P. F. Hlava, B. Mckenzie, and G. L. Zender, *J. Electrochem. Soc.*, **144**, 2621 (1997).
  13. R. G. Buchheit, M. A. Martinez, and L. P. Montes, *J. Electrochem. Soc.*, **147**, 119 (2000).
  14. Q. Meng and G. S. Frankel, *J. Electrochem. Soc.*, **151**, B271 (2004).
  15. Y. Yoon, Ph.D. Thesis, The Ohio State University, Columbus, OH (2004).
  16. T. J. R. Leclere and R. C. Newman, *J. Electrochem. Soc.*, **149**, B52 (2002).
  17. R. G. Buchheit, L. P. Montes, M. A. Martinez, J. Micheal, and P. F. Hlava, *J. Electrochem. Soc.*, **146**, 4424 (1999).
  18. R. G. Buchheit and R. K. Boger, *Localized Corrosion*, p. 265, NACE International, Houston, TX (2001).
  19. W. R. McGovern, P. Schmutz, R. G. Buchheit, and R. L. McCreery, *J. Electrochem. Soc.*, **147**, 4494 (2000).
  20. G. Sauerbrey, *Z. Phys.*, **155**, 206 (1959).
  21. Henkel, Materials Safety Data Sheet for Alodine 1200S, Henkel Corporation.
  22. R. G. Buchheit, *J. Electrochem. Soc.*, **142**, 3994 (1995).
  23. Q. J. Meng and G. S. Frankel, *Surf. Interface Anal.*, **36**, 30 (2004).
  24. W. Zhang, B. L. Hurley, and R. G. Buchheit, *J. Electrochem. Soc.*, **149**, B357 (2002).